Can the gravitational wave background feel wiggles in spacetime?

Ye, G.; Silvestri, A.

The Astrophysical Journal Letters, 963:L15 (8pp), 2024 March 1 https://doi.org/10.3847/2041-8213/ad2851

Can the Gravitational Wave Background Feel Wiggles in Spacetime?

Gen Ye and Alessandra Silvestri
Institute Lorentz, Leiden University, P.O. Box 9506, Leiden 2300 RA, The Netherlands; ye@lorentz.leidenuniv.nl
Received 2023 November 8; revised 2024 January 8; accepted 2024 February 8; published 2024 February 22

Abstract

Recently the international pulsar timing array collaboration has announced the first strong evidence for an isotropic gravitational-wave background (GWB). We propose that rapid small oscillations (wiggles) in the Hubble parameter would trigger a resonance with the propagating gravitational waves, leaving unique signatures in the GWB spectrum as sharp resonance peaks/troughs. The proposed signal can appear at all frequency ranges and is common to GWBs with arbitrary origin. The resonant signal can appear as a trough only when the GWB is primordial, and its amplitude will also be larger by one perturbation order than in the nonprimordial case. These properties serve as a smoking gun for the primordial origin of the observed GWB. We showcased the viability of the signal to near future observations using the recent NANOGrav 15 yr data.

Unified Astronomy Thesaurus concepts: Gravitational wave astronomy (675); Gravitational waves (678); Cosmology (343); Cosmological evolution (336)

1. Introduction and Conclusion

A common-spectrum red noise (noise whose power spectrum decreases with increasing frequency) shared between pulsars has been reported in 2020 (Arzoumanian et al. 2020; Chen et al. 2021; Goncharov et al. 2021). Recently, multiple pulsar timing array (PTA) collaborations, NANOGrav (Agazie et al. 2023a), EPTA (Antoniadis et al. 2023a), PPTA (Reardon et al. 2023), and CPTA (Xu et al. 2023) have announced detection of Hellings–Downs like spatial correlation (Hellings & Downs 1983) in this common-spectrum signal at 3σ–4σ, which indicates that such a signal is highly likely to be the first detection of an isotropic gravitational-wave background (GWB).

Due to the weakness of the gravitational interaction, gravitational waves (GWs), and the GWB as well, are thought to be insensitive to any environmental physics they propagate through, unless such physics has strength beyond the linear regime, which is typically only true near the GW source. As a result, most theoretical studies of the PTA signal have focused on the possible sources such as supermassive black holes (see Agazie et al. 2023b; Antoniadis et al. 2023b for some up-to-date constraints, and also Huang et al. 2023; Konoplya & Zhidenko 2023; Yang et al. 2023b), inflation (Starobinsky 1979; Rubakov et al. 1982; Guzzetti et al. 2016; Vagnozzi 2021, 2023; Borah et al. 2023; Choudhury 2023; Datta 2023; Firouzjahi & Talebian 2023; Niu & Rahat 2023; Unal et al. 2023), scalar-induced GWs (Tomita 1967; Matarrese et al. 1993, 1994; Domènech 2021; Abe & Tada 2023; Cai et al. 2023; Ebadi et al. 2023; Franciolini et al. 2023; Liu et al. 2023a; Wang et al. 2023a; Yi et al. 2023; Zhu et al. 2023), and collision of bubbles of first-order phase transitions (Kosowsky et al. 1992; Caprini et al. 2008; Huber & Konstandin 2008; Arzoumanian et al. 2021; Li et al. 2021; Ashoorioon et al. 2022; Addazi et al. 2023; Bringmann et al. 2023; Cruz et al. 2023; Du et al. 2023; Fujikura et al. 2023; Megias et al. 2023; Xiao et al. 2023; Yang et al. 2023a; Zu et al. 2023), as well as the leftover topological defects (Vilenkin 1985; Hindmarsh & Kibble 1995; Damour & Vilenkin 2005; Saikawa 2017; Wang et al. 2023b; Bai et al. 2023; Blasi et al. 2023; Ellis et al. 2023; Gouttenoire & Vitagliano 2023; Kitajima et al. 2023; Lazarides et al. 2023; Li 2023; Lu & Chiang 2023; Servant & Simakachorn 2023) and magnetic fields (Roper Pol et al. 2022; Li et al. 2023; see Caprini & Figueroa 2018 for a review; see Antoniadis et al. 2023b; Afzal et al. 2023; Bian et al. 2023 for some updated constraints). Very few, on the other hand, consider the propagation effect. Expansion of the Universe on cosmological timescales can influence the broad shape (tilt) of the isotropic GWB spectrum, whose effect, however, is highly degenerate with the assumptions on the unknown details of the sources (see, e.g., Agazie et al. 2023b; Antoniadis et al. 2023b; Liu et al. 2023b). Propagation through large-scale structure (Camera & Nishizawa 2013; Garoffolo et al. 2020; Garoffolo 2022) and resonance with local fields (Degollado & Herdeiro 2014; Yoshida & Soda 2018; Jung et al. 2020; Tsutsui & Nishizawa 2023) might also imprint anisotropy (unobserved by now) in the GWB.

Contrary to the previously mentioned belief, in this Letter we show that background evolution not only modifies the broad shape of the isotropic GWB spectrum, but also is able to imprint a *localized* signature within reach of near-future experiments. The proposed signature is a resonant peak/trough at $k_c = k_{\rm osc}/2$ in the GWB spectrum induced by rapid small oscillations (wiggles) with wavenumber $k_{\rm osc}$ of the background spacetime $\mathcal{H}$ on top of its slowly varying part $\langle\mathcal{H}\rangle \equiv \bar{\mathcal{H}}$, i.e.,

$$\mathcal{H} = \langle\mathcal{H}\rangle + \mathcal{H}_{\rm osc} \equiv \bar{\mathcal{H}}(1 + \delta_{\rm osc}), \qquad \delta_{\rm osc} < 1, \tag{1}$$

where $\langle\cdot\rangle$ stands for averaging over the rapid oscillation periods. We make no assumptions on the possible physics that sources $\delta_{\rm osc}$, except for that the GW is luminal and weakly coupled (which is expected in General Relativity as well as many theories of dark energy/modified gravity). $\delta_{\rm osc}$ evades most cosmological observations because only the averaging effect on cosmological timescales is constrained and the effect of background on the sub-Hubble process is generally suppressed by powers of $\mathcal{H}/k_{\rm osc}$ without resonance. Even for the most precise cosmic probe, i.e., cosmic microwave background (CMB), it is shown that nonnegligible oscillatory early dark energy (EDE) is allowed by current observation around recombination (Poulin et al. 2019). To the best of our knowledge, searching for the proposed resonant signature in the GWB spectrum is the only known method to detect sub-Hubble background spacetime oscillations, possibly sourced by various mechanisms such as early dark energy/modified gravity (Doran & Robbers 2006; Karwal & Kamionkowski 2016; Poulin et al. 2019; Braglia et al. 2020; Zumalacarregui 2020), in broad energy scales. In particular, this method allows us to constrain spacetime oscillation from the energy scale $T \sim 10^9$ GeV (LIGO) down to $T \sim 0.1$ eV (CMB B-mode). Because the radiation-dominated Universe is transparent to GWs, it opens up a new window on the dynamics of the Universe long before last scattering that would otherwise be hard to constrain due to the thermal equilibrium. The resonance mechanism is general and will therefore also influence the scalar sector. Near recombination, it may generate potentially observable contributions in the CMB power spectrum as was shown recently in Smith et al. (2023). In this work, we focus on the signatures in the tensor sector.

The resonance mechanism applies to GWBs with arbitrary origin, but the strength and shape of the corresponding signature depend on the latter. It is found that a resonant trough is only possible when the GWB is primordial, and its amplitude will also be larger by one perturbation order than in the nonprimordial case. Both properties can serve as a smoking gun for the primordial origin of the GWB. The viability of the signal to near-future observations is showcased using the NANOGrav 15 yr data.

2. GW Resonance

We start from the propagation equation for a GW mode $\gamma(\tau, k)$ on the homogeneous and isotropic cosmological background

$$\ddot{\gamma} + 2\Gamma\dot{\gamma} + k^2\gamma = 0, \tag{2}$$

where upper dots indicate derivation with respect to the conformal time τ. Here we have promoted the Hubble friction $\mathcal{H}$ to a general friction term Γ that can additionally include possible contributions from modified gravity. We assume that the speed of tensors is luminal. In parallel to Equation (1), we can split Γ into a part $\bar{\Gamma}$ slowly varying on cosmological timescales plus fast oscillating wiggles $\delta_{\rm osc}$ with $k_{\rm osc} \gg \mathcal{H}$

$$\Gamma = \bar{\Gamma}(1 + \delta_{\rm osc}), \qquad \delta_{\rm osc} < 1. \tag{3}$$

As discussed in detail in the Appendix, such wiggles can be sourced in early-dark-energy-like scenarios characterized by a canonical scalar field with a ϕ^4 potential.

For oscillations of small amplitude, i.e., $\delta_{\rm osc} < 1$, Equation (2) can be solved perturbatively:

$$\ddot{\gamma}^{(n)} + 2\bar{\Gamma}\dot{\gamma}^{(n)} + k^2\gamma^{(n)} = -2\delta_{\rm osc}\bar{\Gamma}\dot{\gamma}^{(n-1)}, \quad n = 0, 1, ... \qquad \gamma^{(-1)} = 0. \tag{4}$$

We will focus on epochs with a constant equation of state w and assume $\bar{\Gamma} \simeq \bar{\mathcal{H}} = \frac{2}{3w+1}\tau^{-1}$; in this case, the two homogeneous solutions of Equation (2) are $\gamma_1^{(0)} \simeq \frac{J_\nu(k\tau)}{(k\tau)^\nu}$, $\gamma_2^{(0)} \simeq \frac{Y_\nu(k\tau)}{(k\tau)^\nu}$, $\nu = \frac{3(1-w)}{2(1+3w)}$. The leading order correction term $\gamma^{(1)}$ can be found via the Green's function method:

$$\begin{aligned}\gamma^{(1)}(\tau) &= \int_{\tau_i}^{\tau} -2\delta_{\rm osc}\bar{\Gamma}\dot{\gamma}^{(0)}(\tilde{\tau}) \\ &\quad\times \frac{\gamma_1^{(0)}(\tilde{\tau})\gamma_2^{(0)}(\tau) - \gamma_2^{(0)}(\tilde{\tau})\gamma_1^{(0)}(\tau)}{\gamma_1^{(0)}(\tilde{\tau})\dot{\gamma}_2^{(0)}(\tilde{\tau}) - \dot{\gamma}_1^{(0)}(\tilde{\tau})\gamma_2^{(0)}(\tilde{\tau})} d\tilde{\tau} \\ &\simeq \int_{\tau_i}^{\tau} 2\frac{\tilde{\tau}^q}{\tau^q}\bar{\Gamma}\delta_{\rm osc}\frac{\dot{\gamma}^{(0)}(\tilde{\tau})}{k}\sin[k(\tilde{\tau} - \tau)]d\tilde{\tau}, \\ q &= \frac{2}{1+3w},\end{aligned} \tag{5}$$

where in the second line we substituted in the homogeneous solution of $\gamma^{(0)}$ and took the subhorizon limit by keeping only terms with the highest power in $k\tau$.

The leading order correction, $\gamma^{(1)}$, is generally highly suppressed by both the sub-Hubble parameter $\bar{\mathcal{H}}/k$ as well as rapid oscillations. However, it can get amplified if $\delta_{\rm osc}$ oscillates in resonance with $\gamma^{(0)}$, in which case its amplitude at resonance will be determined by $|\delta_{\rm osc}|$, *regardless of* $\bar{\mathcal{H}}/k$. To see this, let us introduce the ansatz

$$\delta_{\rm osc} = \psi_0 \sin(k_{\rm osc}\tau + \alpha), \tag{6}$$

for the wiggles with ψ_0 characterizing the amplitude of $\delta_{\rm osc}$. The leading order GW with conformal wavenumber k can be expressed as $\gamma^{(0)} \simeq \gamma_0 \sin(k\tau + \beta)/(k\tau)^q$. α and β are arbitrary phases. Now the second line of Equation (5) becomes

$$\begin{aligned}\gamma^{(1)}(k) &\simeq \frac{4}{1+3w}\frac{\gamma_0\psi_0}{(k\tau)^q}\int_{\tau_i}^{\tau}\frac{1}{\tilde{\tau}}\sin(k_{\rm osc}\tilde{\tau} + \alpha) \\ &\quad\times\cos(k\tilde{\tau} + \beta)\sin(k(\tilde{\tau} - \tau))d\tilde{\tau} \\ &\simeq \psi_0 f(\Delta k)\frac{\gamma_0\cos(k\tau + \alpha - \beta)}{(k\tau)^q},\end{aligned} \tag{7}$$

where we have used the rapid oscillation approximation $\int_{\tau_i}^{\tau} g(\tilde{\tau})\sin(k\tilde{\tau})d\tilde{\tau} \sim \int_{\tau_i}^{\tau} g(\tilde{\tau})\cos(k\tilde{\tau})d\tilde{\tau} \sim \mathcal{O}(1/k(\tau - \tau_i)) \to 0$ when $k(\tau - \tau_i) \gg 1$ and $\dot{g}/g \ll k$, which is true for sub-Hubble GWs propagating over cosmological distances. Resonance happens at $k_c = k_{\rm osc}/2$ and $f(\Delta k)$ characterizes the shape of the resonant peak with $\Delta k \equiv k - k_c$. For $\Delta k/k \ll 1$, one has the analytic approximation

$$f(\Delta k) \sim \frac{1}{1+3w}[\mathrm{Ci}(2|\Delta k|\tau) - \mathrm{Ci}(2|\Delta k|\tau_i)], \tag{8}$$

where $\mathrm{Ci}(x) \equiv -\int_x^\infty dt\cos(t)/t$ is the cosine integral function. In particular $f(0) = \frac{\log(\tau/\tau_i)}{1+3w} = \frac{\log(a/a_i)}{2} = \frac{N}{2}$, corresponding to one-half of the number of e-folds, N, the Universe underwent from the beginning of the resonance at τ_i. Specializing to the PTA frequency nHz, if resonance starts at horizon reentry ($k \sim 10^{-9}$ Hz $\sim 10^5$ Mpc^{-1}) and continues all the way to radiation-matter equality ($k_{\rm eq} \sim 10^{-2}$ Mpc^{-1}), we get $N \simeq 16$ and $f(0) \simeq 8$.

Usually when comparing with observations, the more relevant quantity is the GW energy density spectrum (Boyle

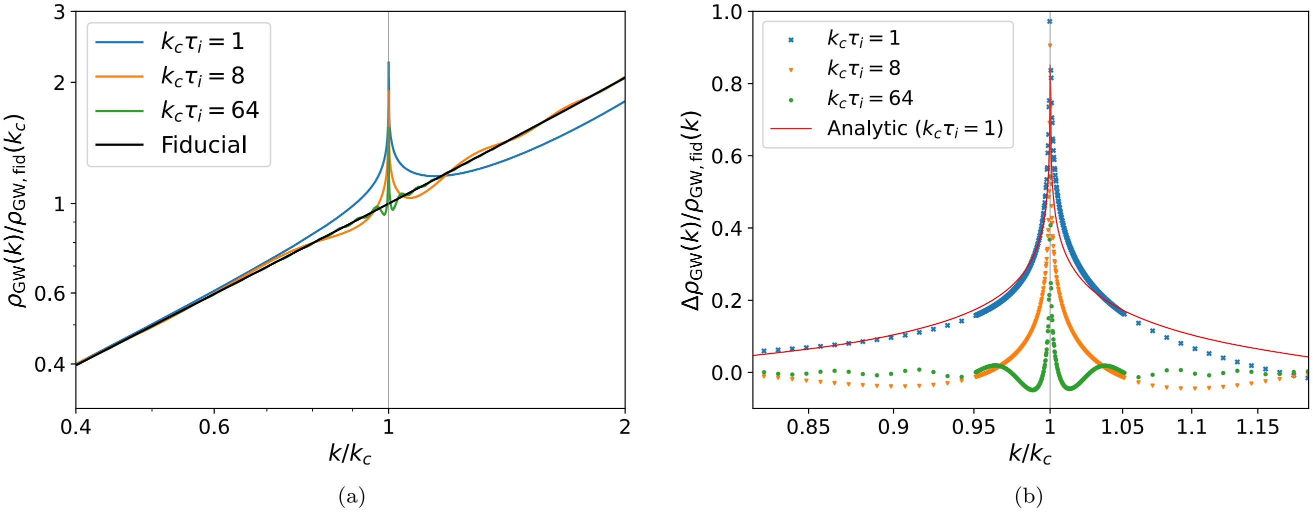

Figure 1. Full numerical results of the energy spectrum of GW with and without (fiducial) resonance for different resonance starting times $k_c\tau_i$. The amplitude of the background wiggle is $\psi_0 = 0.1$. A scale-invariant initial GW spectrum and radiation dominance are assumed. In panel (b) we plot the analytic approximation, from the second line of Equations (9) and (8), of the highest peak (i.e., the $k_c\tau_i = 1$ case) as a red solid line for comparison.

& Steinhardt 2008):

$$\begin{aligned}\rho_{GW}(k) \equiv \frac{d\rho_{GW}}{d\ln k} &= \frac{M_p^2}{4}\frac{k^3}{2\pi^2}\left(\left|\frac{d\gamma}{dt}\right|^2 + \frac{k^2}{a^2}|\gamma|^2\right)\\ &\simeq [1 + 2f(\Delta k)\psi_0\sin(2\beta - \alpha) + f^2(\Delta k)\psi_0^2]\\ &\times\frac{M_p^2}{8\pi^2}\frac{k^3}{a^2\tau^2}.\end{aligned} \tag{9}$$

To arrive at the second line, we assumed that only the leading order correction is important, i.e., $\gamma \simeq \gamma^{(0)} + \gamma^{(1)}$ and used the approximation Equation (7). The term linear in ψ_0 arises from the fact that $\gamma^{(1)}$ is sourced by $\gamma^{(0)}$. There are two physical limits of interest concerning the phase factor $\sin(2\beta - \alpha)$:

1. *Completely random phase.* If the GWB is of sub-Hubble origin, such as supermassive black hole binaries or bubble/topological defect collision after inflation, the phases β of GWs generally satisfy a uniform random distribution. In this case the linear correction term vanishes when summing over all β phases, i.e., $\frac{1}{2\pi}\int_0^{2\pi}\rho_{\rm GW}d\beta$, and the leading order correction is $\mathcal{O}(\psi_0^2)$.
2. *Completely aligned phase.* If the GWB undergoes a horizon reentry mechanism, such as primordial tensor perturbations generated during inflation, the GWs will have exactly the same phase $\beta \sim \pi/2$ due to the adiabatic initial condition. α depends on the actual physics that sources the wiggles $\delta_{\rm osc}$, thus can take arbitrary values in general, e.g., for the explicit example in the Appendix, $|\alpha| \sim \pi/2$ and $|\sin(2\beta - \alpha)| \sim 1$. Therefore, we argue here the phase factor in this case does not vanish and that the leading order correction is $\mathcal{O}(\psi_0)$.

Assuming a completely aligned phase, Figure 1 plots the numeric results of the energy spectrum $\rho_{\rm GW}$, defined by the first line of Equation (9). For the case of $k_c\tau_i = 1$ we plot also the corresponding analytic approximation from the second line of Equation (9), using Equation (8). One can notice that the analytic approximation is able to capture the overall shape of the peak, with the peak height slightly smaller than the numerical result. This is to be expected because $\gamma^{(n)}$, $n \geqslant 2$ are also important at resonance. It is clear from Figure 1 that the peak width is affected by $k_c\tau_i$. The more sub-Hubble the GW is when resonance starts, the narrower the peak width, though the peak height only depends on how long the resonance lasts logarithmically, through the e-folding number N. This implies higher frequency resolution would be required if the resonance starts when the GW is deep sub-Hubble. We will come back to this issue in the next section. It is worth noting here that the signal strength is higher by one perturbation order (ψ_0) in the aligned phase case and a resonant trough (negative phase factor) is *only* possible in this case; see the Appendix for a concrete example. Therefore, observation of a resonant trough will immediately imply primordial origin (part) of the GWB. The difference between a peak and a trough is equivalent to taking $\psi_0 \to -\psi_0$; thus, without loss of generality, we will always assume a peak hereafter for better presentation.

A unique property of the resonance signal is that it is sensitive to the origin of the GWB, as explained in the previous paragraph. In particular, a trough is only possible when GWB is primordial. To further illustrate this point, we promote the phase of GWs to a Gaussian random variable with different variance and compute the phase-averaged GWB energy spectrum. The results are plotted in Figure 2, interpolating between a resonance trough with amplitude $\mathcal{O}(\psi_0)$ to a small peak of order $\mathcal{O}(\psi_0^2)$. GWB of primordial origin falls into the "completely aligned phase" case, corresponding to *phase variance* = 0. On the other hand, when the GWB originates from many individual and uncorrelated subhorizon sources, it falls in the "completely random phase" case, corresponding to *phase variance* = ∞ (i.e., uniform distribution).

3. Resonant GW and PTA

Experiments have finite frequency resolution and measure integrated power in frequency bins. An important property of the integrated signal is that it is insensitive to how long the resonance lasts, i.e., the e-folding number N, as long as it is long enough (i.e., $k_c\tau \gg 1$ and $\tau/\tau_i \gg 1$). This property can be seen by analytically integrating Equation (8) over a frequency

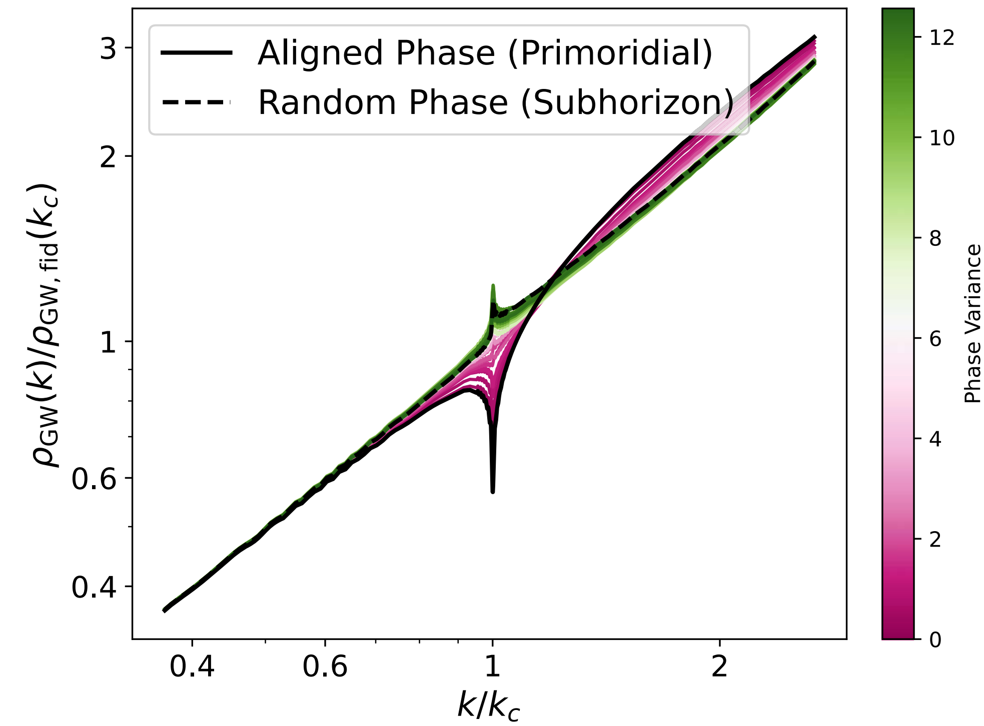

Figure 2. Resonance signal in the GW energy spectrum with a color coding for the variance of the random phase factor. "Completely aligned phase" corresponds to phase variance $= 0$ (reddish color), while "completely random phase" corresponds to phase variance $\to \infty$ (greenish color).

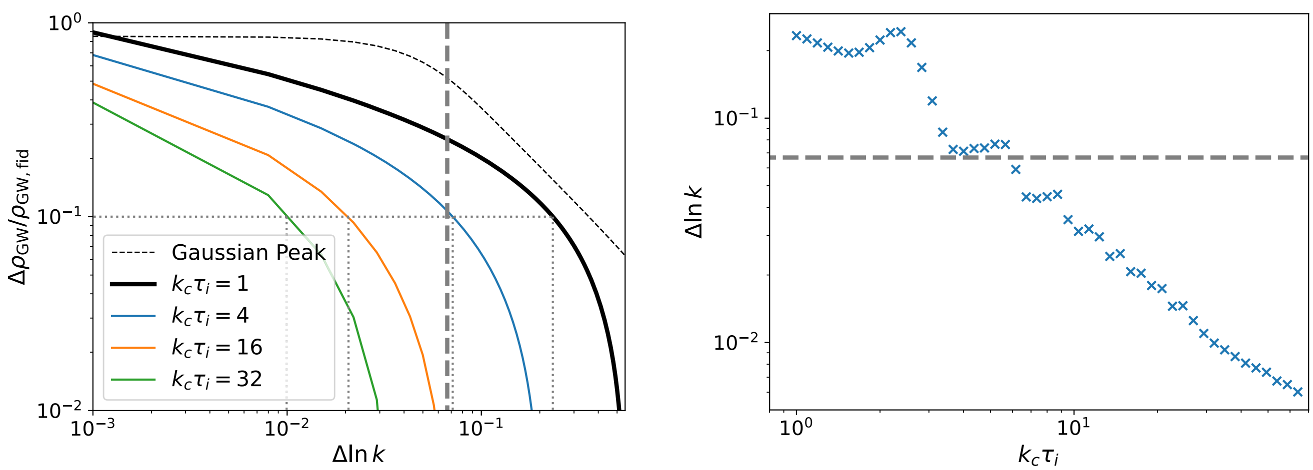

(a) (b)

Figure 3. Integrated power excess signal $\frac{\Delta\rho_{\mathrm{GW}}}{\rho_{\mathrm{GW,fid}}}$ induced by GW resonance with background wiggles of amplitude $\psi_0 = 0.1$, in the logarithmic frequency bin centered at k_c. NANOGrav 15 yr data detect possible GWB signal up to bin 8 (Agazie et al. 2023a), corresponding to the max frequency resolution $\Delta \ln k \simeq \ln(8/7)/2 \simeq 0.07$, which is indicated by dashed gray lines in the plots. The black dashed line in the left panel indicates the result for a Gaussian peak with the same peak height and half-width as the $k\tau_i = 1$ resonant peak (thick black solid line).

bin of width $\lambda \equiv \frac{\Delta k_{\max}}{k_c}$:

$$\frac{\int_{|\Delta k|<\lambda k_c} k^3 f(\Delta k)\, d\ln k}{\int_{|\Delta k|<\lambda k_c} k^3 d\ln k} \simeq \frac{1}{1+3w}\left[-\mathrm{Ci}(2\lambda k_c\tau_i) + \frac{\sin(2\lambda k_c\tau_i)}{2\lambda k_c\tau_i}\right] + \mathcal{O}\!\left(\frac{1}{k_c\tau}\right), \quad (10)$$

which is independent of N. The bin width λ should satisfy $(k_c\tau)^{-1} < \lambda \ll 1$ for the approximation to hold. The explicit dependence on $k_c\tau_i$ also explains what we see in Figure 1 regarding the peak width. The resonance peak is very narrow; to assess the viability of Equation (9) in observations, we plot the relation between log frequency resolution $\Delta \ln k \equiv \ln(1+\lambda)$ and the signal as integrated power excess $\Delta\rho_{\mathrm{GW}}/\rho_{\mathrm{GW,fid}} \equiv (\rho_{\mathrm{GW}} - \rho_{\mathrm{GW,fid}})/\rho_{\mathrm{GW,fid}}$ in the frequency bin $[e^{-\Delta \ln k}k_c,\, e^{\Delta \ln k}k_c]$ in Figure 3. Due to the sharpness of the resonant peak/trough, see Figure 1, the integrated power excess has a unique frequency resolution dependence as compared to smooth peaks, i.e., the solid and dashed lines in Figure 3, which could be used to distinguish the resonance signal from other possible local signatures. As already

Table 1
Parameter Priors for the MCMC Analysis

Parameter	Prior
$\log_{10} A_{\rm GWB}$	Uniform[−18, −6]
$\gamma_{\rm GW}$	Uniform[0, 7]
f_c [nHz]	Uniform[3, 30]
ψ_0	Uniform[−1, 1]

mentioned in the previous section, higher frequency resolution is needed to resolve the signal if resonance starts deep sub-Hubble. To see this, we plot in Figure 3 the required frequency resolution $\Delta \ln k$ to reach 10% power excess signal for different resonance starting times $k_c\tau_i$. According to Figure 3, for a detector with 10% energy precision, the relative frequency resolution needs to be above 40% (note the actual bin size is $2\Delta \ln k$) in order to resolve the resonant signal sourced by wiggles $\delta_{\rm osc}$ of order 10%. For PTA experiments, if the spectrum is binned with bin width $1/T_{\rm obs}$, $T_{\rm obs}$ being the observation time span, 40% relative resolution can be reached for bin number $i \geqslant 3$.

Assuming the most optimistic situation, where the resonance starts immediately after horizon reentry, i.e., $k_c\tau_i = 1$, and $|\sin(2\beta - \alpha)| = 1$, we propose the following resonant GW signal template for PTA:

$$\Omega_{\rm GW}(k) = \frac{2\pi^2}{3}\left(\frac{{\rm yr}^{-1}}{H_0}\right)^2 \times [1 + \psi_0 F_{\Delta k}(k, k_c)] A_{\rm GWB}^2 \left(\frac{k/2\pi}{{\rm yr}^{-1}}\right)^{5-\gamma_{\rm GWB}}, \tag{11}$$

where Δk is the width of the frequency bin used and k_c (f_c) is the resonance wavenumber (frequency). Typically, $\Delta k \simeq 2\pi/T_{\rm obs}$. The shape function F is defined as

$$F_{\Delta k}(k, k_c) \equiv \frac{\int_{k-\Delta k/2}^{k+\Delta k/2} \tilde{k}^{1.8} f(\tilde{k} - k)\, d\ln\tilde{k}}{\int_{k-\Delta k/2}^{k+\Delta k/2} \tilde{k}^{1.8}\, d\ln\tilde{k}}, \tag{12}$$

where the factor $k^{1.8}$ comes from setting $\gamma_{\rm GWB} = 3.2$ according to NANOGrav GWB best fit (Agazie et al. 2023a) so that $\Omega_{\rm GW}(k) \propto k^{1.8}$ and $f(\Delta k)$ are approximated by Equation (8). We fit the template Equation (11) to the public NANOGrav 15 yr data (Agazie et al. 2023c) using the Monte Carlo Markov Chain (MCMC) method, with $\Delta k = 2\pi/16.03$yr as described in the Letter. The priors are summarized in Table 1, in which resonance frequency f_c is confined to the region where GWB has been observed (Agazie et al. 2023a). Figure 4 shows the MCMC posterior distributions of the spectrum parameters $\{\log_{10} A_{\rm GWB}, \gamma_{GWB}, \psi_0, f_c\}$. Current data are not enough to well constrain local features in the spectrum, thus the wide contours in the plot. However, quite interestingly, both the results assuming Hellings–Downs spatial correlation (HD) and common-spectrum uncorrelated red noise (CURN) display a peak in f_c posterior around 15 nHz, hinting at a possible feature there. This peak is significantly higher when CURN is assumed, which leads us to attribute this curiosity to the difference in power excess signal between CURN and HD at frequency bins 6 and 7 (roughly corresponding to $f = 10$–16 nHz) in the NANOGrav results (Agazie et al. 2023a).

4. Final Remarks

Yes, it is possible to detect the resonant signal sourced by spacetime wiggles through PTA. Fitting the template Equation (11) to the recent NANOGrav 15 yr data hints at a curious feature near $f_c \sim 15$ nHz; see Figure 4. It is unclear whether such a feature is due to physics or statistical fluctuations. Further study is needed to evaluate its credibility.

The proposed resonance signal can appear at all frequencies. The next step would be to study its phenomenology and viability in other frequency bands, corresponding to, e.g., ground-based LIGO/Virgo/KAGRA (Aasi et al. 2015; Acernese et al. 2015; Akutsu et al. 2020), space-based LISA (Amaro-Seoane et al. 2017), Taiji (Hu & Wu 2017), and CMB B-mode (Kamionkowski et al. 1997a, 1997b; Ade et al. 2021).

Acknowledgments

G.Y. particularly thanks Alice Garoffolo for insightful discussion during the initial phase of this work and for careful proofread of the draft. PTA data analysis is performed using the `PTArcade` software (Lamb et al. 2023; Mitridate & Wright 2023). Our work is supported by NWO and the Dutch Ministry of Education, Culture and Science (OCW) (grant VI.Vidi.192.069).

Appendix
An Example Model of GW Resonance

In this appendix we demonstrate that wiggles in H can be sourced by an oscillatory canonical scalar field:

$$\mathcal{S} = \int dx^4 \sqrt{-g}\left[\frac{M_p^2}{2}R - \frac{1}{2}(\partial\phi)^2 - \lambda\phi^4\right] + \mathcal{S}_m. \tag{A1}$$

The field is initially frozen at its initial value ϕ_i by Hubble friction when $m_{\rm eff}^2 \sim V_{\phi\phi} \ll H^2$, then thaws at $V_{\phi\phi} \sim H^2$ and undergoes oscillations driven by the potential $V = \lambda\phi^4$ around its minimum. If the thawing time is near matter-radiation equality, such a theory has been shown to be a suitable early dark energy candidate (Agrawal et al. 2019; Ye & Piao 2020), which significantly alleviates the Hubble tension (Karwal & Kamionkowski 2016; Poulin et al. 2019) in a CMB-compatible way, but not fully resolve it (Hill et al. 2020). The quartic potential $V(\phi) = \lambda\phi^4$ is important for our example because it drives the radiation-like oscillations in the scalar field. Specifically, at max field displacement ϕ_0 in one oscillation cycle, one has $V(\phi_0) = \lambda\phi_0^4 \sim \rho_\phi \propto a^{-4}$, which implies $\phi_0 \sim a^{-1}$. At $\phi = 0$ we have $\frac{1}{2}\left(\frac{d\phi}{dt}\right)^2 \sim \phi_0^2 k_{\rm phys}^2/2 \sim \rho_\phi \propto a^{-4}$ implying the physical wavevector $k_{\rm phys} \propto a^{-1}$. Thus, ϕ oscillates with a fixed conformal wavenumber k_ϕ, which is essential for resonance with GW. Neglecting the Hubble friction, we can estimate the oscillation period by $T = 4\int_0^{\phi_0} d\phi \frac{dt}{d\phi} = 4\int_0^{\phi_0} d\phi [2(V(\phi_0) - V(\phi))]^{-1/2} \simeq 3.7\lambda^{-1/2}\phi_0^{-1}$. Together with the thawing condition $9H^2 \simeq V_{\phi\phi}$ (Marsh & Ferreira 2010), one obtains an order-of-magnitude estimation of the oscillatory

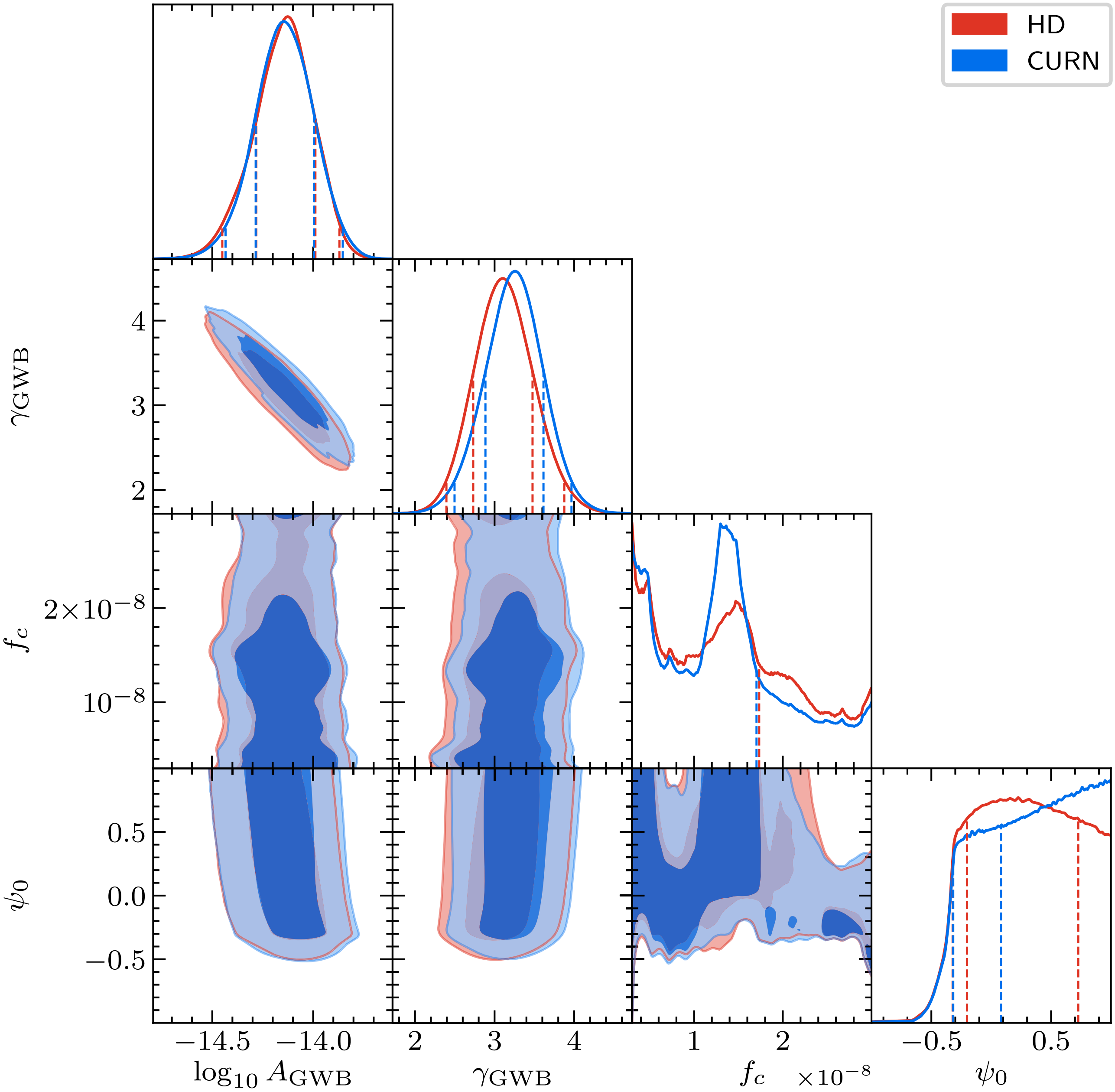

Figure 4. 68% and 95% posterior distributions of the resonance signal template parameters $\{\log_{10}A_{\rm GWB},\ \gamma_{\rm GWB},\ \psi_0,\ f_c\}$ fitted to NANOGrav 15 yr data.

frequency

$$\frac{k_\phi}{\mathcal{H}_i} \sim 3(\lambda f_\phi)^{1/2}, \tag{A2}$$

where we have denoted the conformal Hubble scale at some initial time as $\mathcal{H}_i$ and defined the energy fraction of ϕ as $f_\phi \equiv \rho_{\phi,i}\big/3M_p^2H_i^2 = \lambda(\phi_i/M_p)^4\big/3$, and in the last equality we de-dimensionalize $\lambda \to \lambda H_i^2 M_p^2$. In radiation dominance, $f_\phi =$ conts. Due to time scaling of the scalar field amplitude $\phi \sim a^{-1}$, $\delta_{\rm osc}$ is sourced by ρ_ϕ through the Freedman equation with $k_{\rm osc} = 2k_\phi$, thus resonance at $k_c = k_\phi$, with its amplitude proportional to $(\mathcal{H}/k_\phi)^2$. Therefore, in this case one needs a large f_ϕ to have a sizable effect, which might appear at the onset of reheating or short scalar-dominating phases during radiation dominance. For illustration purposes, we consider $f_\phi = 0.9$ during radiation dominance and solve the cosmic background and tensor equations numerically. The results are plotted in Figure 5. The plotted modes are initially super horizon with the adiabatic initial condition $h = 1, \dot{h} = 0$. We observe a resonance trough, and because in this example the amplitude of $\delta_{\rm osc}$ decays with time, the trough is smoother than that in the main text. For scalar fields, oscillation in ϕ can also trigger parametric resonance in the scalar field perturbations, whose phenomenology in the CMB has been studied in Smith et al. (2023).

ORCID iDs

Gen Ye https://orcid.org/0000-0002-0172-1147
Alessandra Silvestri https://orcid.org/0000-0001-6904-5061

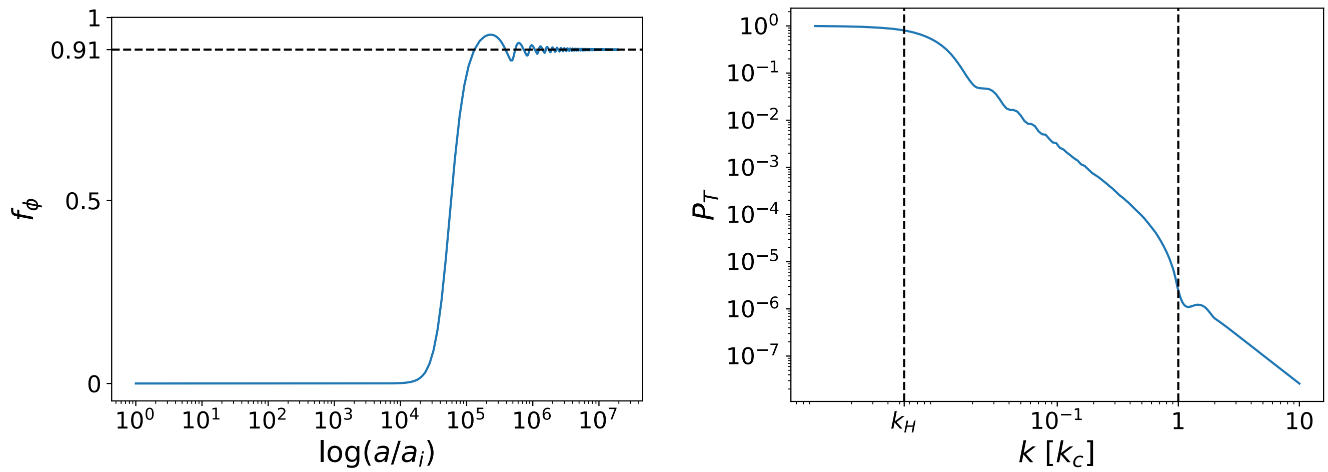

(a) (b)

Figure 5. Numeric results of theory (A1). (a) Scalar field energy fraction. (b) Tensor power spectrum. Vertical dashed lines in panel (b) mark the position of resonance k_c and the conformal Hubble scale k_H at which the spectrum is plotted.

References

Aasi, J., Abbott, B.P., Abbott, R., et al. 2015, CQGra, 32, 074001
Akutsu, T., Ando, M., Arai, K., et al. 2020, PTEP, 2021, 05A103
Abe, K. T., & Tada, Y. 2023, PhRvD, 108, 101304
Acernese, F., Agathos, M., Agatsuma, K., et al. 2015, CQGra, 32, 024001
Addazi, A., Cai, Y.-F., Marciano, A., & Visinelli, L. 2023, PhRvD, 109, 015028
Ade, P. A. R., Ahmed, Z., Amiri, M., et al. 2021, PhRvL, 127, 151301
Afzal, A., Agazie, G., Anumarlapudi, A., et al. 2023, ApJL, 951, L11
Agazie, G., Anumarlapudi, A., Archibald, Anne M., et al. 2023a, ApJL, 951, L8
Agazie, G., Anumarlapudi, A., Archibald, Anne M., et al. 2023b, ApJL, 952, L37
Agazie, G., Alam, M., Anumarlapudi, A., et al. 2023c, ApJL, 951, L9
Agrawal, P., Cyr-Racine, F.-Y., Pinner, D., & Randall, L. 2019, PDU, 42, 101347
Amaro-Seoane, P., Audley, H., Babak, S., et al. 2017, arXiv:1702.00786
Antoniadis, J., Arumugam, P., Arumugam, S., et al. 2023a, A&A, 678, A50
Antoniadis, J., Arumugam, P., Arumugam, S., et al. 2023b, arXiv:2306.16227
Arzoumanian, Z., Baker, P., Blumer, H., et al. 2020, ApJL, 905, L34
Arzoumanian, Z., Baker, P., Blumer, H., et al. 2021, PhRvL, 127, 251302
Ashoorioon, A., Rezazadeh, K., & Rostami, A. 2022, PhLB, 835, 137542
Bai, Y., Chen, T.-K., & Korwar, M. 2023, JHEP, 2023, 194
Bian, L., Ge, S., Shu, J., et al. 2023, arXiv:2307.02376
Blasi, S., Mariotti, A., Rase, A., & Sevrin, A. 2023, JHEP, 2023, 169
Borah, D., Jyoti Das, S., & Samanta, R. 2023, arXiv:2307.00537
Boyle, L. A., & Steinhardt, P. J. 2008, PhRvD, 77, 063504
Braglia, M., Ballardini, M., Emond, W. T., et al. 2020, PhRvD, 102, 023529
Bringmann, T., Depta, P. F., Konstandin, T., Schmidt-Hoberg, K., & Tasillo, C. 2023, JCAP, 2023, 053
Cai, Y.-F., He, X.-C., Ma, X., Yan, S.-F., & Yuan, G.-W. 2023, SciBu, 68, 2929
Camera, S., & Nishizawa, A. 2013, PhRvL, 110, 151103
Caprini, C., Durrer, R., & Servant, G. 2008, PhRvD, 77, 124015
Caprini, C., & Figueroa, D. G. 2018, CQGra, 35, 163001
Chen, S., Caballero, R. N., Guo, Y. J., et al. 2021, MNRAS, 508, 4970
Choudhury, S. 2023, arXiv:2307.03249
Cruz, J. S., Niedermann, F., & Sloth, M. S. 2023, PhLB, 846, 138202
Damour, T., & Vilenkin, A. 2005, PhRvD, 71, 063510
Datta, S., & Samanta, R. 2023, PhRvD, 108, 091706
Degollado, J. C., & Herdeiro, C. A. R. 2014, PhRvD, 90, 065019
Domènech, G. 2021, Univ, 7, 398
Doran, M., & Robbers, G. 2006, JCAP, 06, 026
Du, X. K., Huang, M. X., Wang, F., & Zhang, Y. K. 2023, arXiv:2307.02938
Ebadi, R., Kumar, S., McCune, A., Tai, H., & Wang, L.-T. 2023, arXiv:2307.01248
Ellis, J., Lewicki, M., Lin, C., & Vaskonen, V. 2023, PhRvD, 108, 103511
Firouzjahi, H., & Talebian, A. 2023, JCAP, 2023, 032
Franciolini, G., Iovino, J. A., Vaskonen, V., & Veermae, H. 2023, PhRvL, 131, 201401
Fujikura, K., Girmohanta, S., Nakai, Y., & Suzuki, M. 2023, PhLB, 846, 138203
Garoffolo, A. 2022, arXiv:2210.05718
Garoffolo, A., Tasinato, G., Carbone, C., Bertacca, D., & Matarrese, S. 2020, JCAP, 11, 040
Goncharov, B., Shannon, R. M., Reardon, D. J., et al. 2021, ApJL, 917, L19
Gouttenoire, Y., & Vitagliano, E. 2023, arXiv:2306.17841
Guzzetti, M. C., Bartolo, N., Liguori, M., & Matarrese, S. 2016, NCimR, 39, 399
Hellings, R., & Downs, G. s. 1983, ApJL, 265, L39
Hill, J. C., McDonough, E., Toomey, M. W., & Alexander, S. 2020, PhRvD, 102, 043507
Hindmarsh, M. B., & Kibble, T. W. B. 1995, RPPh, 58, 477
Hu, W.-R., & Wu, Y.-L. 2017, Natl. Sci. Rev., 4, 685
Huang, H.-L., Cai, Y., Jiang, J.-Q., Zhang, J., & Piao, Y.-S. 2023, arXiv:2306.17577
Huber, S. J., & Konstandin, T. 2008, JCAP, 09, 022
Jung, S., Kim, T., Soda, J., & Urakawa, Y. 2020, PhRvD, 102, 055013
Kamionkowski, M., Kosowsky, A., & Stebbins, A. 1997a, PhRvD, 55, 7368
Kamionkowski, M., Kosowsky, A., & Stebbins, A. 1997b, PhRvL, 78, 2058
Karwal, T., & Kamionkowski, M. 2016, PhRvD, 94, 103523
Kitajima, N., Lee, J., Murai, K., Takahashi, F., & Yin, W. 2023, arXiv:2306.17146
Konoplya, R. A., & Zhidenko, A. 2023, arXiv:2307.01110
Kosowsky, A., Turner, M. S., & Watkins, R. 1992, PhRvD, 45, 4514
Lamb, W. G., Taylor, S. R., & van Haasteren, R. 2023, PhRvD, 108, 103019
Lazarides, G., Maji, R., & Shafi, Q. 2023, PhRvD, 108, 095041
Li, H.-H., Ye, G., & Piao, Y.-S. 2021, PhLB, 816, 136211
Li, X.-F. 2023, arXiv:2307.03163
Li, Y., Zhang, C., Wang, Z., et al. 2023, arXiv:2306.17124
Liu, L., Chen, Z.-C., & Huang, Q.-G. 2023a, arXiv:2307.01102
Liu, L., Chen, Z.-C., & Huang, Q.-G. 2023b, JCAP, 2023, 071
Lu, B.-Q., & Chiang, C.-W. 2023, arXiv:2307.00746
Marsh, D. J. E., & Ferreira, P. G. 2010, PhRvD, 82, 103528
Matarrese, S., Pantano, O., & Saez, D. 1993, PhRvD, 47, 1311
Matarrese, S., Pantano, O., & Saez, D. 1994, PhRvL, 72, 320
Megias, E., Nardini, G., & Quiros, M. 2023, PhRvD, 108, 095017
Mitridate, A., & Wright, D. 2023, PTArcade, v0.0.1, Zenodo, doi:10.5281/zenodo.8106173
Niu, X., & Rahat, M. H. 2023, PhRvD, 108, 115023
Poulin, V., Smith, T. L., Karwal, T., & Kamionkowski, M. 2019, PhRvL, 122, 221301
Reardon, D. J., Zic, A., Shannon, R., et al. 2023, ApJL, 951, L6
Roper Pol, A., Caprini, C., Neronov, A., & Semikoz, D. 2022, PhRvD, 105, 123502
Rubakov, V. A., Sazhin, M. V., & Veryaskin, A. V. 1982, PhLB, 115, 189
Saikawa, K. 2017, Univ, 3, 40
Servant, G., & Simakachorn, P. 2023, PhRvD, 108, 123516
Smith, T. L., Giblin, J. T., Amin, M. A., et al. 2023, PhRvD, 108, 123534
Starobinsky, A. A. 1979, JETPL, 30, 682
Tomita, K. 1967, PThPh, 37, 831

Tsutsui, T., & Nishizawa, A. 2023, PhRvD, 107, 103516
Unal, C., Papageorgiou, A., & Obata, I. 2023, arXiv:2307.02322
Vagnozzi, S. 2021, MNRAS, 502, L11
Vagnozzi, S. 2023, JHEAp, 39, 81
Vilenkin, A. 1985, PhR, 121, 263
Wang, S., Zhao, Z.-C., Li, J.-P., & Zhu, Q.-H. 2023a, arXiv:2307.00572
Wang, Z., Lei, L., Jiao, H., Feng, L., & Fan, Y.-Z. 2023b, Science China Physics, Mechanics & Astronomy, 66, 120403
Xiao, Y., Yang, J. M., & Zhang, Y. 2023,
Xu, H., Chen, S., Guo, Y., et al. 2023, RAA, 23, 075024
Jiang, S., Yang, A., Ma, J., & Huang, F. P. 2023a, arXiv:2306.17827
Yang, J., Xie, N., & Huang, F. P. 2023b, arXiv:2306.17113
Ye, G., & Piao, Y.-S. 2020, PhRvD, 101, 083507
Yi, Z., Gao, Q., Gong, Y., Wang, Y., & Zhang, F. 2023, SCPMA, 66, 120404
Yoshida, D., & Soda, J. 2018, IJMPD, 27, 1850096
Wang, S., Zhao, Z.-C., & Zhu, Q.-H. 2023, arXiv:2307.03095
Zu, L., Zhang, C., Li, Y.-Y., et al. 2023, arXiv:2306.16769
Zumalacarregui, M. 2020, PhRvD, 102, 023523